

Slowing and stopping light using an optomechanical crystal array

D.E. Chang^{1,4}, A.H. Safavi-Naeini^{2,4}, M. Hafezi³, O. Painter²

¹Institute for Quantum Information and Center for the Physics of Information, California Institute of Technology, Pasadena, CA 91125

²Thomas J. Watson, Sr., Laboratory of Applied Physics, California Institute of Technology, Pasadena, CA 91125

³Joint Quantum Institute and Department of Physics, University of Maryland, College Park, MD 20742

E-mail: opainter@caltech.edu

Abstract. One of the major advances needed to realize all-optical information processing of light is the ability to delay or coherently store and retrieve optical information in a rapidly tunable manner. In the classical domain, this optical buffering is expected to be a key ingredient to managing the flow of information over complex optical networks. Such a system also has profound implications for quantum information processing, serving as a long-term memory that can store the full quantum information contained in an optical pulse. Here we suggest a novel approach to light storage involving an optical waveguide coupled to an optomechanical crystal array, where light in the waveguide can be dynamically and coherently transferred into long-lived mechanical vibrations of the array. Under realistic conditions, this system is capable of achieving large bandwidths and storage/delay times in a compact, on-chip platform.

PACS numbers: 37.10.Vz, 42.50.Pq, 42.50.Ar, 42.50.Lc, 42.79-e

⁴ These authors contributed equally to this work.

1. Introduction

Light is a natural candidate to transmit information across large networks due to its high speed and low propagation losses. A major obstacle to building more advanced optical networks is the lack of an all-optically controlled device that can robustly delay or store optical wave-packets over a tunable amount of time. In the classical domain, such a device would enable all-optical buffering and switching, bypassing the need to convert an optical pulse to an electronic signal. In the quantum realm, such a device could serve as a memory to store the full quantum information contained in a light pulse until it can be passed to a processing node at some later time.

A number of schemes to coherently delay and store optical information are being actively explored. These range from tunable coupled resonator optical waveguide (CROW) structures [1, 2], where the propagation of light is dynamically altered by modulating the refractive index of the system, to electromagnetically induced transparency (EIT) in atomic media [3, 4], where the optical pulse is reversibly mapped into internal atomic degrees of freedom. While these schemes have been demonstrated in a number of remarkable experiments [5, 6, 7, 8], they remain difficult to implement in a practical setting. Here, we present a novel approach to store or stop an optical pulse propagating through a waveguide, wherein coupling between the waveguide and a nearby nano-mechanical resonator array enables one to map the optical field into long-lived mechanical excitations. This process is completely quantum coherent and allows the delay and release of pulses to be rapidly and all-optically tuned. Our scheme combines many of the best attributes of previously proposed approaches, in that it simultaneously allows for large bandwidths of operation, on-chip integration, relatively long delay/storage times, and ease of external control. Beyond light storage, this work opens up the intriguing possibility of a platform for quantum or classical all-optical information processing using mechanical systems.

2. Description of system: an optomechanical crystal array

An optomechanical crystal [9] is a periodic structure that constitutes both a photonic [10] and a phononic [11] crystal. The ability to engineer optical and mechanical properties in the same structure should enable unprecedented control over light-matter interactions. Planar two-dimensional (2D) photonic crystals, formed from patterned thin dielectric films on the surface of a microchip, have been successfully employed as nanoscale optical circuits capable of efficiently routing, diffracting, and trapping light. Fabrication techniques for such 2D photonic crystals have matured significantly over the last decade, with experiments on a Si chip [12] demonstrating excellent optical transmission through long ($N > 100$) linear arrays of coupled photonic crystal cavities. In a similar Si chip platform it has recently been shown that suitably designed photonic crystal cavities also contain localized acoustic resonances which are strongly coupled to the optical field via radiation pressure [9]. These planar optomechanical crystals (OMCs) are thus a natural

candidate for implementation of our proposed slow-light scheme.

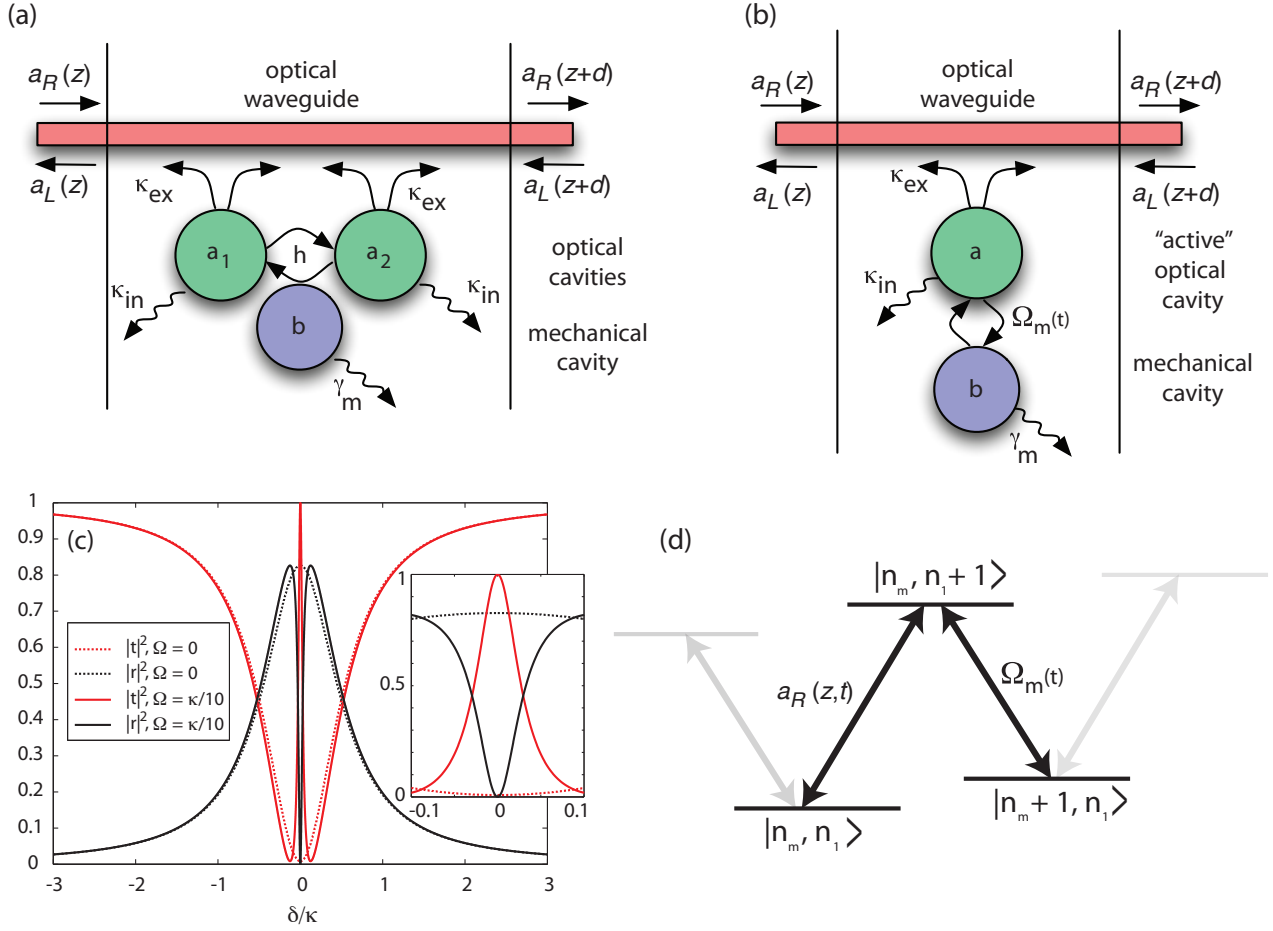


Figure 1. (a) Illustration of a double optical cavity system forming the unit cell of the optomechanical array. A two-way optical waveguide is coupled to a pair of optical cavity modes a_1 and a_2 , whose resonance frequencies differ by the frequency of the mechanical mode b . Both optical modes leak energy into the waveguide at a rate κ_{ex} and have an inherent decay rate κ_{in} . The mechanical resonator optomechanically couples the two optical resonances with a cross coupling rate of h . (b) A simplified system diagram where the classically driven cavity mode a_2 is effectively eliminated to yield an optomechanical driving amplitude Ω_m between the mechanical mode and cavity mode a_1 . (c) Frequency-dependent reflectance (black curve) and transmittance (red) of a single array element, in the case of no optomechanical driving amplitude $\Omega_m = 0$ (dotted line) and an amplitude of $\Omega_m = \kappa_{\text{ex}}/10$ (solid line). The inherent cavity decay is chosen to be $\kappa_{\text{in}} = 0.1\kappa_{\text{ex}}$. (inset) The optomechanical coupling creates a transparency window of width $\sim 4\Omega_m^2/\kappa_{\text{ex}}$ for a single element and enables perfect transmission on resonance, $\delta_k = 0$. (d) Energy level structure of simplified system. The number of photons and phonons are denoted by n_1 and n_m , respectively. The optomechanical driving amplitude Ω_m couples states $|n_m + 1, n_1\rangle \leftrightarrow |n_m, n_1 + 1\rangle$ while the light in the waveguide couples states $|n_m, n_1\rangle \leftrightarrow |n_m, n_1 + 1\rangle$. The two couplings create a set of Λ -type transitions analogous to that in EIT.

In the following we consider an optomechanical crystal containing a periodic array of

such defect cavities (see figures 1(a),(b)). Each element of the array contains two optical cavity modes (denoted 1, 2) and a co-localized mechanical resonance. The Hamiltonian describing the dynamics of a single element is of the form

$$\tilde{H}_{\text{om}} = \hbar\omega_1\hat{a}_1^\dagger\hat{a}_1 + \hbar\omega_2\hat{a}_2^\dagger\hat{a}_2 + \hbar\omega_m\hat{b}^\dagger\hat{b} + \hbar h \left(\hat{b} + \hat{b}^\dagger \right) \left(\hat{a}_1^\dagger\hat{a}_2 + \hat{a}_2^\dagger\hat{a}_1 \right). \quad (1)$$

Here $\omega_{1,2}$ are the resonance frequencies of the two optical modes, ω_m is the mechanical resonance frequency, and $\hat{a}_1, \hat{a}_2, \hat{b}$ are annihilation operators for these modes. The optomechanical interaction cross-couples the cavity modes 1 and 2 with a strength characterized by h and that depends linearly on the mechanical displacement $\hat{x} \propto (\hat{b} + \hat{b}^\dagger)$. While we formally treat $\hat{a}_1, \hat{a}_2, \hat{b}$ as quantum mechanical operators, for the most part it also suffices to treat these terms as dimensionless classical quantities describing the positive-frequency components of the optical fields and mechanical position. In addition to the optomechanical interaction described by equation (1), the cavity modes 1 are coupled to a common two-way waveguide (described below). Each element is decoupled from the others except through the waveguide.

The design considerations necessary to achieve such a system are discussed in detail in the section “Optomechanical crystal design.” For now, we take as typical parameters $\omega_1/2\pi = 200$ THz, $\omega_m/2\pi = 10$ GHz, $h/2\pi = 0.35$ MHz, and mechanical and (unloaded) optical quality factors of $Q_m \equiv \omega_m/\gamma_m \sim 10^3$ (room temperature)- 10^5 (low temperature) and $Q_1 \equiv \omega_1/\kappa_{1,\text{in}} = 3 \times 10^6$, where γ_m is the mechanical decay rate and $\kappa_{1,\text{in}}$ is the intrinsic optical cavity decay rate. Similar parameters have been experimentally observed in other OMC systems [9, 13]. In practice, one can also over-couple cavity mode 1 to the waveguide, with a waveguide-induced optical decay rate κ_{ex} that is much larger than κ_{in} .

For the purpose of slowing light, the cavity modes 2 will be resonantly driven by an external laser, so that to good approximation $\hat{a}_2 \approx \alpha_2(t)e^{-i\omega_2 t}$ can be replaced by its mean-field value. We furthermore consider the case where the frequencies are tuned such that $\omega_1 = \omega_2 + \omega_m$. Keeping only the resonant terms in the optomechanical interaction, we arrive at a simplified Hamiltonian for a single array element (see figure 1(b)),

$$H_{\text{om}} = \hbar\omega_1\hat{a}_1^\dagger\hat{a}_1 + \hbar\omega_m\hat{b}^\dagger\hat{b} + \hbar\Omega_m(t) \left(\hat{a}_1^\dagger\hat{b}e^{-i(\omega_1-\omega_m)t} + h.c. \right). \quad (2)$$

Here we have defined an effective optomechanical driving amplitude $\Omega_m(t) = h\alpha_2(t)$ and assume that $\alpha_2(t)$ is real. Mode 2 thus serves as a “tuning” cavity that mediates population transfer (Rabi oscillations) between the “active” cavity mode 1 and the mechanical resonator at a controllable rate $\Omega(t)$, which is the key mechanism for our stopped-light protocol. In the following analysis, we will focus exclusively on the active cavity mode and drop the “1” subscript.

A Hamiltonian of the form (2) also describes an optomechanical system with a single optical mode, when the cavity is driven off resonance at frequency $\omega_1 - \omega_m$ and \hat{a}_1 corresponds to the sidebands generated at frequencies $\pm\omega_m$ around the classical driving field. For a single system, this Hamiltonian leads to efficient optical cooling of the mechanical motion [14, 15], a technique being used to cool nano-mechanical

systems toward their quantum ground states [16, 17, 18, 19]. While the majority of such work focuses on how optical fields affect the mechanical dynamics, here we show that the optomechanical interaction strongly modifies optical field propagation to yield the slow/stopped light phenomenon. Equation (2) is quite general and thus this phenomenon could in principle be observed in any array of optomechanical systems coupled to a waveguide. In practice, there are several considerations that make the 2D OMC “ideal.” First, our system exhibits an extremely large optomechanical coupling h and contains a second optical tuning cavity that can be driven resonantly, which enables large driving amplitudes Ω_m using reasonable input power [20]. Using two different cavities also potentially allows for greater versatility and addressability of our system. For instance, in our proposed design the photons in cavity 1 are spatially filtered from those in cavity 2 [20]. Second, the 2D OMC is an easily scalable and compact platform. Finally, as described below, the high mechanical frequency of our device compared to typical optomechanical systems allows for a good balance between long storage times and suppression of noise processes.

3. Slowing and stopping light

3.1. Static regime

We first analyze propagation in the waveguide when $\Omega_m(t) = \Omega_m$ is static during the transit interval of the signal pulse. As shown in the Appendix, the evolution equations in a rotating frame for a single element located at position z_j along the waveguide are given by

$$\frac{d\hat{a}}{dt} = -\frac{\kappa}{2}\hat{a} + i\Omega_m\hat{b} + i\sqrt{\frac{c\kappa_{\text{ex}}}{2}}(\hat{a}_{R,\text{in}}(z_j) + \hat{a}_{L,\text{in}}(z_j)) + \sqrt{c\kappa_{\text{in}}}\hat{a}_N(z_j), \quad (3)$$

$$\frac{d\hat{b}}{dt} = -\frac{\gamma_m}{2}\hat{b} + i\Omega_m\hat{a} + \hat{F}_N(t). \quad (4)$$

Equation (3) is a standard input relation characterizing the coupling of right- ($\hat{a}_{R,\text{in}}$) and left-propagating ($\hat{a}_{L,\text{in}}$) optical input fields in the waveguide with the cavity mode. Here $\kappa = \kappa_{\text{ex}} + \kappa_{\text{in}}$ is the total optical cavity decay rate, $\hat{a}_N(z)$ is quantum noise associated with the inherent optical cavity loss, and for simplicity we have assumed a linear dispersion relation $\omega_k = c|k|$ in the waveguide. Equation (4) describes the optically driven mechanical motion, which decays at a rate γ_m and is subject to thermal noise $\hat{F}_N(t)$. The cavity mode couples to the right-propagating field through the equation

$$\left(\frac{1}{c}\frac{\partial}{\partial t} + \frac{\partial}{\partial z}\right)\hat{a}_R(z, t) = i\sqrt{\frac{\kappa_{\text{ex}}}{2c}}\delta(z - z_j)\hat{a} + ik_0\hat{a}_R, \quad (5)$$

where $k_0 = \omega_1/c$. We solve the above equations to find the reflection and transmission coefficients r, t of a single element for a right-propagating incoming field of frequency ω_k (see Appendix). In the limit where $\gamma_m = 0$, and defining $\delta_k \equiv \omega_k - \omega_1$,

$$r(\delta_k) = -\frac{\delta_k\kappa_{\text{ex}}}{\delta_k(-2i\delta_k + \kappa) + 2i\Omega_m^2}, \quad (6)$$

while $t = 1 + r$. Example reflectance and transmittance curves are plotted in figure 1(c). For any non-zero Ω_m , a single element is perfectly transmitting on resonance, whereas for $\Omega_m = 0$ resonant transmission past the cavity is blocked. When $\Omega_m \neq 0$, excitation of the cavity mode is inhibited through destructive interference between the incoming field and the optomechanical coupling. In EIT, a similar effect occurs via interference between two electronic transitions. This analogy is further elucidated by considering the level structure of our optomechanical system (figure 1(d)), where the interference pathways and the “ Λ ”-type transition reminiscent of EIT are clearly visible. The interference is accompanied by a steep phase variation in the transmitted field around resonance, which can result in a slow group velocity. These steep features and their similarity to EIT in a single optomechanical system have been theoretically [21, 22] and experimentally studied [23, 24], while interference effects between a single cavity mode and two mechanical modes have also been observed [25]. From r, t for a single element, the propagation characteristics through an infinite array (figure 2(a)) can be readily obtained via band structure calculations [10]. To maximize the propagation bandwidth of the system, we choose the spacing d between elements such that $k_0 d = (2n + 1)\pi/2$ where n is a non-negative integer. With this choice of phasing the reflections from multiple elements destructively interfere under optomechanical driving. Typical band structures are illustrated in figures 2(b)-(f). The color coding of the dispersion curves (red for waveguide, green for optical cavity, blue for mechanical resonance) indicates the distribution of energy or fractional occupation in the various degrees of freedom of the system in steady-state. Far away from the cavity resonance, the dispersion relation is nearly linear and simply reflects the character of the input optical waveguide, while the propagation is strongly modified near resonance ($\omega = \omega_1 = \omega_2 + \omega_m$). In the absence of optomechanical coupling ($\Omega_m = 0$), a transmission band gap of width $\sim \kappa$ forms around the optical cavity resonance (reflections from the bare optical cavity elements constructively interfere). In the presence of optomechanical driving, the band gap splits in two (blue shaded regions) and a new propagation band centered around the cavity resonance appears in the middle of the band gap. For weak driving ($\Omega_m \lesssim \kappa$) the width of this band is $\sim 4\Omega_m^2/\kappa$, while for strong driving ($\Omega_m \gtrsim \kappa$) one recovers the “normal mode splitting” of width $\sim 2\Omega_m$ [26]. This relatively flat polaritonic band yields the slow-light propagation of interest. Indeed, for small Ω_m the steady-state energy in this band is almost completely mechanical in character, indicating the strong mixing and conversion of energy in the waveguide to mechanical excitations along the array.

It can be shown that the Bloch wavevector near resonance is given by (see Appendix)

$$k_{\text{eff}} \approx k_0 + \frac{\kappa_{\text{ex}} \delta_k}{2d\Omega_m^2} + \frac{i\kappa_{\text{ex}}\kappa_{\text{in}}\delta_k^2}{4d\Omega_m^4} + \frac{(2\kappa_{\text{ex}}^3 - 3\kappa_{\text{ex}}\kappa_{\text{in}}^2 + 12\kappa_{\text{ex}}\Omega_m^2)\delta_k^3}{24d\Omega_m^6}. \quad (7)$$

The group velocity on resonance, $v_g = (dk_{\text{eff}}/d\delta_k)^{-1}|_{\delta_k=0} = 2d\Omega_m^2/\kappa_{\text{ex}}$ can be dramatically slowed by an amount that is tunable through the optomechanical coupling strength Ω_m . The quadratic and cubic terms in k_{eff} characterize pulse absorption and group velocity dispersion, respectively. In the relevant regime where $\kappa_{\text{ex}} \gg \kappa_{\text{in}}, \kappa_{\text{ex}} \gtrsim \Omega_m$,

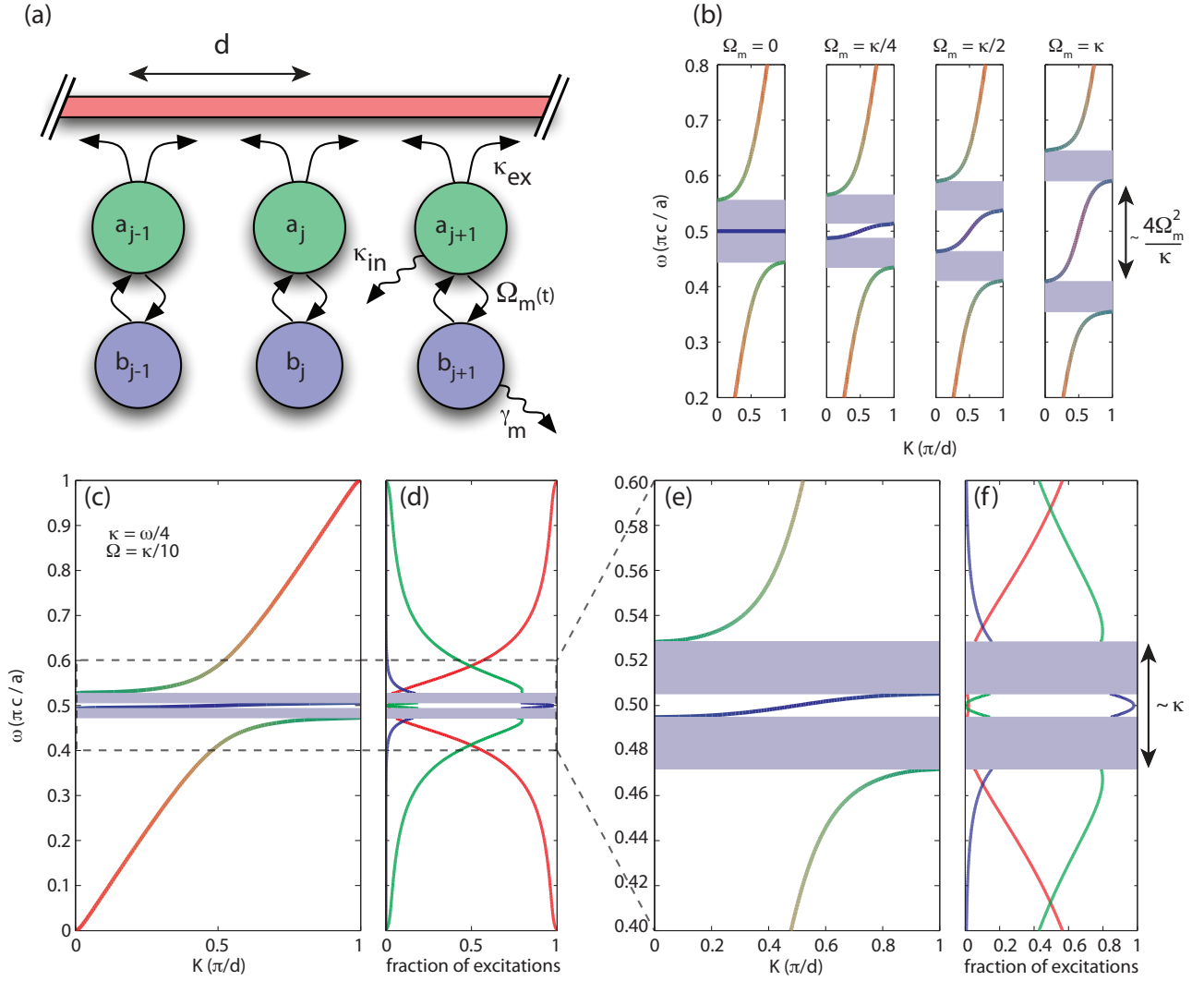


Figure 2. (a) Illustration of an optomechanical crystal array. A two-way optical waveguide is coupled to a periodic array of optomechanical elements spaced by a distance d . The optical cavity modes a_j of each element leak energy into the waveguide at a rate κ_{ex} and have an inherent decay rate κ_{in} . The mechanical resonator of each element has frequency ω_m and is optomechanically coupled to the cavity mode through a tuning cavity (shown in figure 1) with strength Ω_m . (b) The band structure of the system, for a range of driving strengths between $\Omega_m = 0$ and $\Omega_m = \kappa$. The blue shaded regions indicate band gaps, while the color of the bands elucidates the fractional occupation (red for energy in the optical waveguide, green for the optical cavity, and blue for mechanical excitations). The dynamic compression of the bandwidth is clearly visible as $\Omega_m \rightarrow 0$. (c) Band structure for the case $\Omega_m = \kappa/10$ is shown in greater detail. (d) The fractional occupation for each band in (c) is plotted separately. It can be seen that the polaritonic slow-light band is mostly mechanical in nature, with a small mixing with the waveguide modes and negligible mixing with the optical cavity mode. Zoom-ins of figures (c) and (d) are shown in (e) and (f).

these effects are negligible within a bandwidth $\Delta\omega \sim \min\left(\frac{2\sqrt{2}\Omega_m^2}{\sqrt{N\kappa_{\text{ex}}\kappa_{\text{in}}}}, \frac{2(6\pi)^{1/3}\Omega_m^2}{\kappa_{\text{ex}}N^{1/3}}\right)$. The second term is the bandwidth over which certain frequency components of the pulse acquire a π -phase shift relative to others, leading to pulse distortion. This yields a bandwidth-delay product of

$$\Delta\omega\tau_{\text{delay}} \sim \min\left(\sqrt{2N\kappa_{\text{ex}}/\kappa_{\text{in}}}, (6\pi N^2)^{1/3}\right) \quad (8)$$

for static Ω_m and negligible mechanical losses. When intrinsic optical cavity losses are negligible, and if one is not concerned with pulse distortion, light can propagate over the full bandwidth $\sim 4\Omega_m^2/\kappa$ of the slow-light polariton band and the bandwidth-delay product increases to $\Delta\omega\tau_{\text{delay}} \sim N$ (see Appendix). On the other hand, we note that if we had operated in a regime where $k_0d = \pi n$, constructive interference in reflection would limit the bandwidth-delay product to $\Delta\omega\tau_{\text{delay}} \sim 1$, independent of system size.

In the static regime, the bandwidth-delay product obtained here is analogous to CROW systems [2]. In the case of EIT, a static bandwidth-delay product of $\Delta\omega\tau_{\text{delay}} \sim \sqrt{\text{OD}}$ results, where OD is the optical depth of the atomic medium. This product is limited by photon absorption and re-scattering into other directions, and is analogous to our result $\Delta\omega\tau_{\text{delay}} \sim \sqrt{N\kappa_{\text{ex}}/\kappa_{\text{in}}}$ in the case of large intrinsic cavity linewidth. On the other hand, when κ_{in} is negligible, photons are never lost and reflections can be suppressed by interference. This yields an improved scaling $\Delta\omega\tau_{\text{delay}} \sim N^{2/3}$ or $\sim N$, depending on whether one is concerned with group velocity dispersion. In atomic media, the weak atom-photon coupling makes achieving $\text{OD} > 100$ very challenging [27]. In contrast, in our system as few as $N \sim 10$ elements would be equivalently dense.

3.2. Storage of optical pulse

We now show that the group velocity $v_g(t) = 2d\Omega_m^2(t)/\kappa_{\text{ex}}$ can in fact be adiabatically changed once a pulse is completely localized inside the system, leading to distortion-less propagation at a dynamically tunable speed. In particular, by tuning $v_g(t) \rightarrow 0$, the pulse can be completely stopped and stored.

This phenomenon can be understood in terms of the static band structure of the system (figure 2) and a “dynamic compression” of the pulse bandwidth. The same physics applies for CROW structures [1, 28], and the argument is re-summarized here. First, under constant Ω_m , an optical pulse within the bandwidth of the polariton band completely enters the medium. Once the pulse is inside, we consider the effect of a gradual reduction in $\Omega_m(t)$. Decomposing the pulse into Bloch wavevector components, it is clear that each Bloch wavevector is conserved under arbitrary changes of Ω_m , as it is fixed by the system periodicity. Furthermore, transitions to other bands are negligible provided that the energy levels are varied adiabatically compared to the size of the gap, which translates into an adiabatic condition $|(d/dt)(\Omega_m^2/\kappa)| \lesssim \kappa^2$. Then, conservation of the Bloch wavevector implies that the bandwidth of the pulse is dynamically compressed, and the reduction in slope of the polariton band (figure 2) causes the pulse to propagate

at an instantaneous group velocity $v_g(t)$ without any distortion. In the limit that $\Omega_m \rightarrow 0$, the polaritonic band becomes flat and completely mechanical in character, indicating that the pulse has been reversibly and coherently mapped onto stationary mechanical excitations within the array. We note that since Ω_m is itself set by the tuning cavities, its rate of change cannot exceed the optical linewidth and thus the adiabaticity condition is always satisfied in the weak-driving regime.

The maximum storage time is set by the mechanical decay rate, $\sim 1/\gamma_m$. For realistic system parameters $\omega_m/2\pi = 10$ GHz and $Q_m = 10^5$, this yields a storage time of ~ 10 μ s. In CROW structures, light is stored as circulating fields in optical nano-cavities, where state of the art quality factors of $Q \sim 10^6$ limit the storage time to ~ 1 ns. The key feature of our system is that we effectively “down-convert” the high-frequency optical fields to low-frequency mechanical excitations, which naturally decay over much longer time scales. While storage times of ~ 10 ms are possible using atomic media [29], their bandwidths so far have been limited to < 1 MHz [28]. In our system, bandwidths of ~ 1 GHz are possible for realistic circulating powers in the tuning cavities.

3.3. Imperfections in storage

The major source of error in our device will be mechanical noise, which through the optomechanical coupling can be mapped into noise power in the optical waveguide output. In our system, mechanical noise emerges via thermal fluctuations and Stokes scattering (corresponding to the counter-rotating terms in the optomechanical interaction that we omitted from Equation (2)). To analyze these effects, it suffices to consider the case of static Ω_m , and given the linearity of the system, no waveguide input (such that the output will be purely noise). For a single array element, the optomechanical driving Ω_m results in optical cooling of the mechanical motion [14, 15], with the mechanical energy E_m evolving as (see Appendix)

$$\frac{dE_m}{dt} = -\gamma_m (E_m - \hbar\omega_m \bar{n}_{\text{th}}) - \Gamma_{\text{opt}} E_m + \Gamma_{\text{opt}} \frac{\kappa^2}{\kappa^2 + 16\omega_m^2} (E_m + \hbar\omega_m). \quad (9)$$

The first term on the right describes equilibration with the thermal surroundings, where $\bar{n}_{\text{th}} = (e^{\hbar\omega_m/k_B T_b} - 1)^{-1}$ is the Bose occupation number at the mechanical frequency and T_b is the bath temperature. The second (third) term corresponds to cooling (heating) through anti-Stokes (Stokes) scattering, with a rate proportional to $\Gamma_{\text{opt}} = 4\Omega_m^2/\kappa$. The Stokes process is suppressed relative to the anti-Stokes in the limit of good sideband resolution $\kappa/\omega_m \ll 1$. For an array of N elements, a simple upper bound for the output noise power at one end of the waveguide is given by $P_{\text{noise}} = (1/2)(\Gamma_{\text{opt}} E_{ss})N(\omega_1/\omega_m)(\kappa_{\text{ex}}/\kappa)$, where E_{ss} is the steady-state solution of Equation (9). The factor of $1/2$ accounts for the optical noise exiting equally from both output directions, $\Gamma_{\text{opt}} E_{ss}$ is the optically-induced mechanical energy dissipation rate, and $\kappa_{\text{ex}}/\kappa$ describes the waveguide coupling efficiency. The term ω_1/ω_m represents the transduction of mechanical to optical energy and is essentially the price that one pays for down-converting optical excitations to mechanical to yield longer storage times

– in turn, any mechanical noise gets “up-converted” to optical energy (whereas the probability of having a thermal optical photon is negligible). In the relevant regime where $\Gamma_{\text{opt}} \gg \gamma_m$,

$$P_{\text{noise}} \approx \frac{N\hbar\omega_1}{2} \frac{\kappa_{\text{ex}}}{\kappa} \left(\gamma_m \bar{n}_{\text{th}} + \Gamma_{\text{opt}} \left(\frac{\kappa}{4\omega_m} \right)^2 \right). \quad (10)$$

This noise analysis is valid only in the weak-driving regime ($\Omega_m \lesssim \kappa$) [14, 15]. The strong driving regime, where the mechanical motion acquires non-thermal character [32] and can become entangled with the optical fields [33], will be treated in future work.

At room temperature, $\bar{n}_{\text{th}} \approx k_B T_b / \hbar\omega_m$ is large and thermal noise will dominate, yielding a noise power of ~ 0.4 nW per element for previously given system parameters and $\kappa_{\text{ex}}/\kappa \approx 1$. This is independent of Γ_{opt} provided that $\Gamma_{\text{opt}} \gg \gamma_m$, which reflects the fact that all of the thermal heating is removed through the optical channel. For high temperatures, the thermal noise scales inversely with ω_m , and the use of high-frequency mechanical oscillators ensures that the noise remains easily tolerable even at room temperature.

Thermal noise in the high-frequency oscillator can essentially be eliminated in cryogenic environments, which then enables faithful storage of single photons. Intuitively, a single-photon pulse can be stored for a period only as long as the mechanical decay time $\sim \gamma_m^{-1}$, and as long as a noise-induced mechanical excitation is unlikely to be generated over a region covering the pulse length and over the transit time τ_{delay} . The latter condition is equivalent to the statement that the power $P_{\text{ph}} \sim \hbar\omega_1 \Delta\omega$ in the single-photon pulse exceeds P_{noise} . While we have focused on the static regime thus far, when thermal heating is negligible, realizing $P_{\text{ph}}/P_{\text{noise}} \gtrsim 1$ in the static case in fact ensures that the inequality holds even when $\Gamma_{\text{opt}}(t)$ is time-varying. Physically, the rate of Stokes scattering scales linearly with Γ_{opt} while the group velocity scales inversely, and thus the probability of a noise excitation being added on top of the single-photon pulse is fixed over a given transit length.

In a realistic setting, the optomechanical driving amplitude Ω_m itself will be coupled to the bath temperature, as absorption of the pump photons in the tuning cavities leads to material heating. To understand the limitations as a quantum memory, we have numerically optimized the static bandwidth-delay product $\Delta\omega\tau_{\text{delay}}$ for a train of single-photon pulses, subject to the constraints $\Delta\omega < \min(2\sqrt{2}\Omega_m^2/\sqrt{N\kappa_{\text{ex}}\kappa_{\text{in}}}, 2(6\pi)^{1/3}\Omega_m^2/(\kappa_{\text{ex}}N^{1/3}))$, $P_{\text{ph}}/P_{\text{noise}} > 1$, and $\gamma_m\tau_{\text{delay}} < 1$. As a realistic model for the bath temperature, we take $T_b = T_0 + \chi\alpha_2^2 = T_0 + \chi(\Omega_m/h)^2$, where T_0 is the base temperature and $\chi \sim 2$ μK is a temperature coefficient that describes heating due to pump absorption (see Appendix). Using $T_0 = 100$ mK and $Q_m = 10^5$, we find $(\Delta\omega\tau_{\text{delay}})_{\text{max}} \sim 110$, which is achieved for parameter values $N \sim 275$, $\kappa_{\text{ex}}/2\pi \sim 1.1$ GHz, and $\Omega_m/2\pi \sim 130$ MHz.

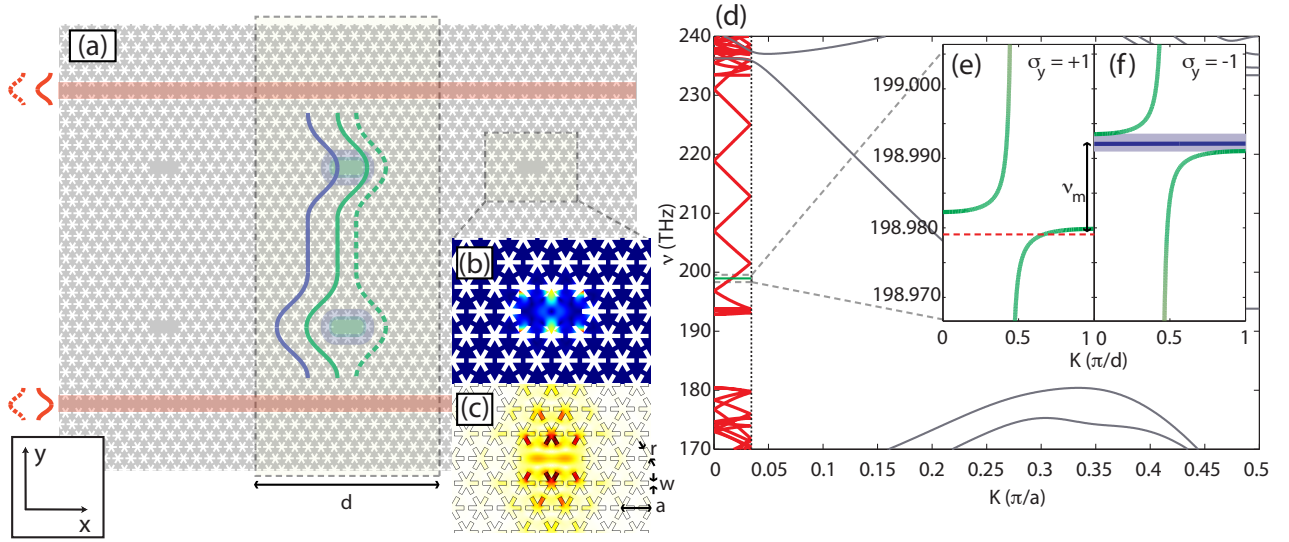


Figure 3. (a) Top view of the proposed optomechanical crystal array, with the superlattice unit-cell of length d highlighted in the center. The unit cell contains two coupled L2 defect cavities (shaded in grey) with two side-coupled linear defect optical waveguides (shaded in red). The different envelope functions pertain to the odd and even optical cavity supermodes (green solid and dashed lines, respectively), the odd mechanical supermode (blue solid line), and the odd and even optical waveguide modes (red solid and dashed lines). The displacement field amplitude $|\mathbf{Q}(\mathbf{r})|$ of the mechanical mode and in-plane electric field amplitude $|\mathbf{E}(\mathbf{r})|$ of the optical mode are shown in (b) and (c), respectively, for a single L2 defect cavity. (d) Bandstructure of the linear-defect waveguide (grey) and the zone folded superlattice of the entire coupled-resonator system (red). The cavity mode (green) crosses the superlattice band at mid-zone, and the waveguide-cavity interaction is shown in more detail in the insets (e) and (a) for the even ($\sigma_y = +1$) and odd ($\sigma_y = -1$) supermodes, respectively.

4. Optomechanical crystal design

A schematic showing a few periods of our proposed 2D OMC slow-light structure is given in figure 3. The structure is built around a “snowflake” crystal pattern of etched holes into a Silicon slab [20]. This pattern, when implemented with a physical lattice constant of $a = 400$ nm, snowflake radius $r = 168$ nm, and snowflake width $w = 60$ nm (see figure 3(a)), provides a simultaneous phononic bandgap from 8.6 to 12.6 GHz and a photonic pseudo-bandgap from 180 to 230 THz (see Appendix). Owing to its unique bandgap properties, the snowflake patterning can be used to form waveguides and resonant cavities for both acoustic and optical waves simply by removing regions of the pattern. For instance, a single point defect, formed by removing two adjacent holes (a so-called “L2” defect), yields the co-localized phononic and photonic resonances shown in figures 3(b) and (c), respectively. The radiation pressure, or optomechanical coupling between the two resonances can be quantified by a coupling rate, g , which corresponds to the frequency shift in the optical resonance line introduced by a single phonon of the

mechanical resonance. Numerical finite-element-method (FEM) simulations of the L2 defect indicate the mechanical resonance occurs at $\omega_m/2\pi = 11.2$ GHz, with a coupling rate of $g/2\pi = 489$ kHz to the optical mode at frequency $\omega_o/2\pi = 199$ THz (free-space optical wavelength of $\lambda_0 \approx 1500$ nm).

In order to form the double-cavity system described in the slow-light scheme above, a pair of L2 cavities are placed in the near-field of each other as shown in the dashed box region of figure 3(a). Modes of the two degenerate L2 cavities mix, forming supermodes of the double-cavity system which are split in frequency. The frequency splitting between modes can be tuned via the number of snowflake periods between the cavities. As described in more detail in the Appendix, it is the optomechanical cross-coupling of the odd (\mathbf{E}_-) and even (\mathbf{E}_+) optical supermodes mediated by the motion of the odd parity mechanical supermode (\mathbf{Q}_-) of the double-cavity that drives the slow-light behaviour of the system. Since \mathbf{Q}_- is a displacement field that is antisymmetric about the two cavities, there is no optomechanical self-coupling between the optical supermodes and this mechanical mode. On the other hand, the cross-coupling between the two different parity optical supermodes is large and given by $h = g/\sqrt{2} = 2\pi(346 \text{ kHz})$. By letting \hat{a}_1 , \hat{a}_2 and \hat{b} be the annihilation operators for the modes \mathbf{E}_- , \mathbf{E}_+ and \mathbf{Q}_- , we obtain the system Hamiltonian of equation (1).

The different spatial symmetries of the optical cavity supermodes also allow them to be addressed independently. To achieve this we create a pair of linear defects in the snowflake lattice as shown in figure 3(a), each acting as a single-mode optical waveguide at the desired frequency of roughly 200 THz (see figure 3(d)). Sending light down both waveguides, with the individual waveguide modes either in or out of phase with each other, will then excite the even or odd supermode of the double cavity, respectively. The waveguide width and proximity to the L2 cavities can be used to tune the cavity loading (see Appendix), which for the structure in figure 3(a) results in the desired $\kappa_{\text{ex}}/2\pi = 2.4$ GHz. It should be noted that these line-defect waveguides do not guide phonons at the frequency of \mathbf{Q}_- , and thus no additional phonon leakage is induced in the localized mechanical resonance.

The full slow-light waveguide system consists of a periodic array of the double-cavity, double-waveguide structure. The numerically computed band diagram, for spacing $d = 15a$ periods of the snowflake lattice between cavity elements (the superlattice period), is shown in figure 3(d). This choice of superlattice period results in the folded superlattice band intersecting the \mathbf{E}_- (\hat{a}_1) cavity frequency ω_1 at roughly mid-zone, corresponding to the desired inter-cavity phase shift of $kd = \pi/2$. A zoom-in of the bandstructure near the optical cavity resonances is shown in figures 3(e) and (f). In figure 3(e) the even parity supermode bandstructure is plotted (i.e., assuming the even supermode of the double-waveguide is excited), whereas in figure 3(f) it is the odd parity supermode bandstructure.

A subtlety in the optical pumping of the periodically arrayed waveguide system is that for the \mathbf{E}_+ (\hat{a}_2) optical cavity resonance at ω_2 , there exists a transmission bandgap. In order to populate cavity \hat{a}_2 , then, and to create the polaritonic band

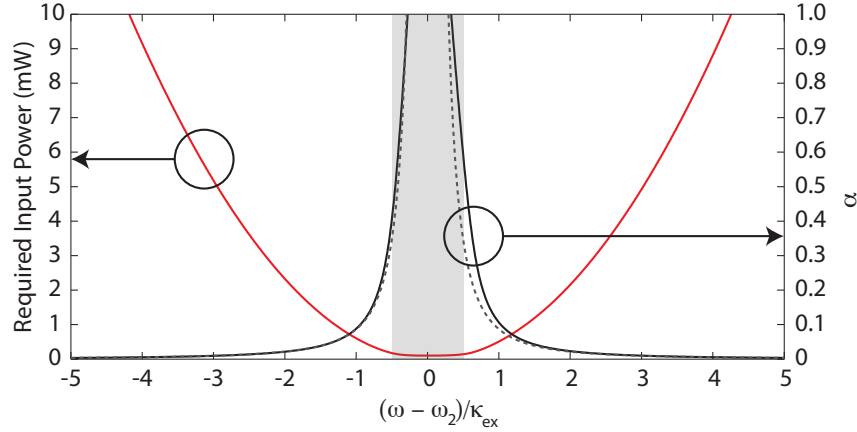


Figure 4. The input power (red line) required to achieve the system parameters used in the text, i.e. $\Omega_m/2\pi = 130$ MHz with $\hbar/2\pi = 0.346$ MHz, and the attenuation per unit cell α (solid black line) are shown as a function of detuning of the pump beam from the pump cavity frequency. The dotted line is the approximate expression derived for the attenuation, $\alpha \approx \kappa_{\text{ex}}\kappa_{\text{in}}/4\delta_k^2$. The grey region indicates the band gap in which the pump cavities cannot be excited from the waveguide. The trade-off between small pump input powers and low pump attenuation factors is readily apparent in this plot.

at ω_1 , the pump beam must be slightly off-resonant from ω_2 , but still at $\omega_1 - \omega_m$. We achieve this by choosing a double-cavity separation (14 periods) resulting in a cavity mode splitting $((\omega_1 - \omega_2)/2\pi = 9.7$ GHz) slightly smaller than the mechanical frequency ($\omega_m/2\pi = 11.2$ GHz), as shown in figures 3(e) and (f). By changing the detuning between $\omega_1 - \omega_2$ and ω_m , a trade-off can be made between the attenuation of the pump beam per unit cell, $\alpha \equiv \exp(-\text{Im}\{K\}d)$, and total required input power, shown in figure 4. In Appendix D.3 we show that the total attenuation per unit cell, is given by $\alpha \approx \kappa_{\text{ex}}\kappa_{\text{in}}/4\delta_k^2$. Interestingly, by using higher input powers such that $\alpha \rightarrow 0$, it is in principle possible to eliminate completely effects due to absorption in the array, which may lead to inhomogeneous pump photon occupations.

5. Outlook

The possibility of using optomechanical systems to facilitate major tasks in classical optical networks has been suggested in several recent proposals [35, 25, 20]. This present work not only extends these prospects, but proposes a fundamentally new direction where optomechanical systems can be used to control and manipulate light at a quantum mechanical level. Such efforts would closely mirror the many proposals to perform similar tasks using EIT and atomic ensembles [4]. At the same time, the optomechanical array has a number of novel features compared to atoms, in that each element can be deterministically positioned, addressed, and manipulated, and a single element is

already optically dense. Furthermore, the ability to freely convert between phonons and photons enables new possibilities for manipulating light through the manipulation of sound. Taken together, this raises the possibility that mechanical systems can provide a novel, highly configurable on-chip platform for realizing quantum optics and “atomic” physics.

6. Acknowledgements

This work was supported by the DARPA/MTO ORCHID program through a grant from AFOSR. DC acknowledges support from the NSF and the Gordon and Betty Moore Foundation through Caltech’s Center for the Physics of Information. ASN acknowledges support from NSERC. M.H. acknowledges support from the U.S. Army Research Office MURI award W911NF0910406.

Appendix A. Equations of motion for optomechanical crystal array

Here we derive the equations of motion for an array of optomechanical systems coupled to a two-way waveguide. Because each element in the array couples independently to the waveguide, it suffices here to only consider a single element, from which the result for an arbitrary number of elements is easily generalized.

We model the interaction between the active cavity mode 1 and the waveguide with the following Hamiltonian,

$$H_{\text{cav-wg}} = \int_{-\infty}^{\infty} dk \hbar (ck - \omega_1) \hat{a}_{R,k}^{\dagger} \hat{a}_{R,k} - \int_{-\infty}^{\infty} dk \hbar (ck + \omega_1) \hat{a}_{L,k}^{\dagger} \hat{a}_{L,k} - \hbar g \sqrt{2\pi} \int_{-\infty}^{\infty} dz \delta(z - z_j) \left(\hat{a}_1^{\dagger} (\hat{a}_R(z) + \hat{a}_L(z)) + h.c. \right). \quad (\text{A.1})$$

Here $\hat{a}_{R,k}, \hat{a}_{L,k}$ are annihilation operators for left- and right-going waveguide modes of wavevector k , and ω_1 is the frequency of the cavity mode. For convenience we have defined all optical energies relative to ω_1 , and assumed that the waveguide has a linear dispersion relation $\omega(k) = c|k|$. The last term on the right describes a point-like coupling between the cavity (at position z_j) and the left- and right-going waveguide modes, with a strength g . The operator $\hat{a}_R(z)$ physically describes the annihilation of a right-going photon at position z and is related to the wavevector annihilation operators by $\hat{a}_R(z) = \frac{1}{\sqrt{2\pi}} \int_{-\infty}^{\infty} dk e^{ikz} \hat{a}_{R,k}$ (with a similar definition for $\hat{a}_L(z)$). Eq. (A.1) resembles a standard Hamiltonian used to formulate quantum cavity input-output relations [36], properly generalized to the case when the cavity accepts an input from either direction. Note that we make the approximation that the left- and right-going waves can be treated as separate quantum fields, with modes in each direction running from $-\infty < k < \infty$. This allows both the left- and right-going fields to separately satisfy canonical field commutation relations, $[\hat{a}_R(z), \hat{a}_R(z')] = [\hat{a}_L(z), \hat{a}_L(z')] = \delta(z - z')$, while commuting with each other. Thus each field contains some unphysical modes (*e.g.*, wavevector components $k < 0$ for the right-going field), but the approximation remains valid as

long as there is no process in the system evolution that allows for the population of such modes.

From the Hamiltonian above, one finds the following Heisenberg equation of motion for the right-going field,

$$\left(\frac{1}{c}\frac{\partial}{\partial t} + \frac{\partial}{\partial z}\right)\hat{a}_R(z) = \frac{\sqrt{2\pi}ig}{c}\delta(z - z_j)\hat{a}_1 + ik_0\hat{a}_R, \quad (\text{A.2})$$

where $k_0 = \omega_1/c$. A similar equation holds for \hat{a}_L . The coupling of the cavity mode to a continuum of waveguide modes leads to irreversible decay of the cavity at a rate κ_{ex} . Below, we will show that κ_{ex} is related to the parameters in the Hamiltonian by $\kappa_{\text{ex}} = 4\pi g^2/c$. With this identification, one recovers Eq. (5) in the main text.

The Heisenberg equation of motion for the cavity mode is given by

$$\frac{d}{dt}\hat{a}_1 = ig\sqrt{2\pi}(\hat{a}_R(z_j) + \hat{a}_L(z_j)). \quad (\text{A.3})$$

To cast this equation into a more useful form, we first integrate the field equation (A.2) across the discontinuity at z_j ,

$$\hat{a}_R(z_j^+) = \hat{a}_R(z_j^-) + \frac{\sqrt{2\pi}ig}{c}\hat{a}_1, \quad (\text{A.4})$$

$$\hat{a}_L(z_j^-) = \hat{a}_L(z_j^+) + \frac{\sqrt{2\pi}ig}{c}\hat{a}_1. \quad (\text{A.5})$$

We can define $\hat{a}_{L,in}(z_j) = \hat{a}_L(z_j^+)$ and $\hat{a}_{R,in}(z_j) = \hat{a}_R(z_j^-)$ as the input fields to the cavity. It then follows that

$$\frac{d}{dt}\hat{a}_1 = ig\sqrt{2\pi}(\hat{a}_{R,in} + \hat{a}_{L,in}) - \frac{2\pi g^2}{c}\hat{a}_1, \quad (\text{A.6})$$

and thus we indeed see that the waveguide induces a cavity decay rate $\kappa_{\text{ex}}/2 = 2\pi g^2/c$. In the case where the cavity has an additional intrinsic decay rate κ_{in} , a similar derivation holds to connect the intrinsic decay with some corresponding noise input field \hat{a}_{in} . From these considerations, and including the opto-mechanical coupling, one arrives at Eq. (3) in the main text,

$$\frac{d\hat{a}_1}{dt} = -\frac{\kappa}{2}\hat{a} + i\Omega_m\hat{b} + i\sqrt{\frac{c\kappa_{\text{ex}}}{2}}(\hat{a}_{R,in}(z_j) + \hat{a}_{L,in}(z_j)) + \sqrt{c\kappa_{\text{in}}}\hat{a}_N(z_j). \quad (\text{A.7})$$

Finally, we consider the equation of motion for the mechanical mode given by Eq. (4) in the main text,

$$\frac{d\hat{b}}{dt} = -\frac{\gamma_m}{2}\hat{b} + i\Omega_m\hat{a}_1 + \hat{F}_N(t). \quad (\text{A.8})$$

The zero-mean noise operator \hat{F}_N must accompany the decay term in the mechanical evolution in order to preserve canonical commutation relations of \hat{b}, \hat{b}^\dagger at all times. In the case where the decay causes the mechanical motion to return to thermal equilibrium with some reservoir at temperature T_b , the noise operator has a two-time correlation function given by $\langle F_N(t)F_N^\dagger(t') \rangle = \gamma_m(\bar{n} + 1)\delta(t - t')$ [37], where $\bar{n} = (e^{\hbar\omega_m/k_B T_b} - 1)^{-1}$ is the Bose occupation number at the mechanical frequency ω_m .

Appendix B. Transfer matrix analysis of propagation

First we derive the reflection and transmission coefficients for a single element in the case of constant opto-mechanical driving amplitude Ω_m . Given the linearity of the system, it suffices to treat Eqs. (A.2), (A.7), and (A.8) as classical equations for this purpose, and furthermore to set the noise terms $\hat{F}_N = 0$, $\hat{a}_{in} = 0$. For concreteness, we will consider the case of an incident right-going cw field in the waveguide. Upon interaction with the opto-mechanical system at z_j , the total right-going field can be written in the form

$$a_R(z) = e^{ikz - i\delta_k t} (\Theta(-z + z_j) + t(\delta_k)\Theta(z - z_j)), \quad (\text{B.1})$$

while the left-going field is given by $a_L(z) = e^{-ikz - i\delta_k t} r(\delta_k)\Theta(-z + z_j)$. Here $\Theta(z)$ is the unit step function, $\delta_k = ck - \omega_1$ is the detuning of the input field from the cavity resonance, and r, t are the reflection and transmission coefficients for the system. At the same time, we look for solutions of the cavity field and mechanical mode of the form $a_1 = Ae^{-i\delta_k t}$ and $b = Be^{-i\delta_k t}$. The coefficients r, t, A, B can be obtained by substituting this ansatz into Eqs. (A.2), (A.7), and (A.8). This yields the reflection coefficient given by Eq. (6) in the main text, while the transmission coefficient is related by $t = 1 + r$.

To calculate propagation through an array of N elements, it is convenient to introduce a transfer matrix formalism. Specifically, the fields immediately to the right of the opto-mechanical element (at $z = z_j^+$) can be related to those immediately to the left (at $z = z_j^-$) in terms of a transfer matrix M_{om} ,

$$\begin{pmatrix} a_R(z_j^+) \\ a_L(z_j^+) \end{pmatrix} = M_{om} \begin{pmatrix} a_R(z_j^-) \\ a_L(z_j^-) \end{pmatrix}, \quad (\text{B.2})$$

where

$$M_{om} = \frac{1}{t} \begin{pmatrix} t^2 - r^2 & r \\ -r & 1 \end{pmatrix}. \quad (\text{B.3})$$

On the other hand, free propagation in the waveguide is characterized by the matrix M_f ,

$$\begin{pmatrix} a_R(z + d) \\ a_L(z + d) \end{pmatrix} = M_f \begin{pmatrix} a_R(z) \\ a_L(z) \end{pmatrix}, \quad (\text{B.4})$$

where

$$M_f = \begin{pmatrix} e^{ikd} & 0 \\ 0 & e^{-ikd} \end{pmatrix}. \quad (\text{B.5})$$

The transfer matrix for an entire system can then be obtained by successively multiplying the transfer matrices for a single element and for free propagation together. In particular, the transfer matrix for a single “block”, defined as interaction with a single opto-mechanical element followed by free propagation over a distance d to the next opto-mechanical element, is given by $M_{block} = M_f M_{om}$, and the propagation over N blocks is simply characterized by $M_N = M_{block}^N$.

Before studying the propagation through the entire array, we first focus on the propagation past two blocks, $M_2 = M_{block}^2$. Because we want our device to be highly transmitting when the optomechanical coupling is turned on, we choose the spacing d between consecutive blocks to be such that $k_0 d = \frac{\pi}{2}(2n + 1)$, where n is an integer. Physically, this spaces consecutive elements by an odd multiple of $\lambda/4$, where λ is the resonant wavelength, such that the reflections from consecutive elements tend to destructively interfere with each other. This can be confirmed by examining the resulting reflection coefficient for the two-block system,

$$r_2 \equiv \frac{M_2(1, 2)}{M_2(2, 2)} = -\frac{\kappa_{\text{ex}}^2 \delta_k^2}{2\Omega_m^4} + O(\delta_k^3), \quad (\text{B.6})$$

where $M_2(i, j)$ denotes matrix elements of M_2 . Note that the reflection coefficient is now suppressed as a quadratic in the detuning, whereas for a single element $r \approx i\kappa_{\text{ex}}\delta_k/2\Omega_m^2$ is linear. In the above equation, we have made the simplifying approximation that $kd \approx k_0 d$, since in realistic systems the dispersion from free propagation will be negligible compared to that arising from interaction with an opto-mechanical element.

Now we can consider transmission past $N/2$ pairs of two blocks (*i.e.*, N elements in total). Because the reflection r_2 is quadratic in the detuning, its effect on the total transmission is only of order δ_k^4 (because the lowest order contribution is an event where the field is reflected twice before passing through the system). Thus, up to $O(\delta_k^3)$, the total transmission coefficient t_N is just given by $t_N \approx t_2^{N/2}$, where $t_2 = 1/M_2(2, 2)$ is the transmission coefficient for a two-block system. It is convenient to write $t_N = e^{ik_{\text{eff}}Nd}$ in terms of an effective wavevector k_{eff} , which leads to Eq. (7) in the main text. Performing a similar analysis for the case where $k_0 d = n\pi$, where reflections from consecutive elements interfere constructively, one finds that the bandwidth-delay product for the system $\Delta\omega\tau_{\text{delay}} \sim 1$ does not improve with the system size.

Appendix C. Optical noise power

In this section we derive the optical cooling equation given by Eq. (9) in the main text. We begin by considering the system Hamiltonian for a single element (Eq. (1) of main text), in the case where the tuning mode 2 is driven on resonance and can be approximated by a classical field, $\hat{a}_2 \rightarrow \alpha_2 e^{-i\omega_2 t}$,

$$\tilde{H}_{om} = \hbar\omega_1 \hat{a}_1^\dagger \hat{a}_1 + \hbar\omega_m \hat{b}^\dagger \hat{b} + \hbar h \left(\hat{b} + \hat{b}^\dagger \right) \left(\hat{a}_1^\dagger \alpha_2 e^{-i\omega_2 t} + \alpha_2^* e^{i\omega_2 t} \hat{a}_1 \right). \quad (\text{C.1})$$

Defining a detuning $\delta_L = \omega_2 - \omega_1$ indicating the frequency difference between the two cavity modes, we can re-write Eq. (C.1) in a rotating frame,

$$\tilde{H}_{om} = -\hbar\delta_L \hat{a}_1^\dagger \hat{a}_1 + \hbar\omega_m \hat{b}^\dagger \hat{b} + \hbar\Omega_m \left(\hat{b} + \hat{b}^\dagger \right) \left(\hat{a}_1 + \hat{a}_1^\dagger \right), \quad (\text{C.2})$$

where $\Omega_m = h\alpha_2$ (we have re-defined the phases such that Ω_m is real). In the weak driving limit ($\Omega_m \lesssim \kappa$), the cavity dynamics can be formally eliminated to arrive at effective optically-induced cooling equations for the mechanical motion [14, 15]. In

particular, the opto-mechanical coupling terms $\hat{a}_1^\dagger \hat{b} + h.c.$ and $\hat{a}_1^\dagger \hat{b}^\dagger + h.c.$ induce anti-Stokes and Stokes scattering, respectively. These processes yield respective optically-induced cooling (Γ_-) and heating (Γ_+) rates

$$\Gamma_{\mp} = \frac{\kappa \Omega_m^2}{(\delta_L \pm \omega_m)^2 + (\kappa/2)^2}. \quad (\text{C.3})$$

In the case where $\delta_L = -\omega_m$, the cooling process is resonantly enhanced by the cavity, yielding a cooling rate $\Gamma_{\text{opt}} \equiv \Gamma_-(\delta_L = -\omega_m) = 4\Omega_m^2/\kappa$ as given in the main text. Also in this case, the optical heating rate is given by $\Gamma_+ = \Gamma_{\text{opt}} \frac{\kappa^2}{\kappa^2 + 16\omega_m^2}$. This leads to the net cooling dynamics given by Eq. (9) in the main text,

$$\frac{dE_m}{dt} = -\gamma_m (E_m - \hbar\omega_m \bar{n}_{th}) - \Gamma_{\text{opt}} E_m + \Gamma_{\text{opt}} \frac{\kappa^2}{\kappa^2 + 16\omega_m^2} (E_m + \hbar\omega_m). \quad (\text{C.4})$$

Because the optical cooling process removes phonons from the mechanical system via optical photons that leak out of the cavity, one can identify $(\omega_1/\omega_m)\Gamma_{\text{opt}}E_m$ as the amount of optical power that is being leaked by the cavity in the anti-Stokes sideband during the cooling process. Similarly, the cavity leaks an amount of power $(\omega_1/\omega_m)\Gamma_{\text{opt}} \frac{\kappa^2}{\kappa^2 + 16\omega_m^2} (E_m + \hbar\omega_m)$ in the Stokes sideband. We have ignored this contribution in Eq. (10) in the main text, because its large frequency separation ($2\omega_m$) from the signal allows it to be filtered out, but otherwise it approximately contributes an extra factor of 2 to the last term in Eq. (10). Finally, we remark that the expression for P_{noise} given by Eq. (10) represents an upper bound in that it does not account for the possibility that the output spectrum from a single element may exceed the transparency bandwidth, which could cause some light to be absorbed within the system after multiple reflections and not make it to the end of the waveguide.

Appendix D. Band structure analysis

Appendix D.1. Derivation of dispersion relation

For simplicity, here we work only with the classical equations so that the intrinsic noise terms in the Heisenberg-Langevin equations can be ignored. We begin by transforming Eqs. (A.7) and (A.8) to the Fourier domain,

$$0 = \left(i\delta_k - \frac{\kappa}{2}\right) a + i\Omega_m b + i\sqrt{\frac{Ck_{\text{ex}}}{2}} (a_{R,in}(z_j) + a_{L,in}(z_j)), \quad (\text{D.1})$$

$$0 = \left(i\delta_k - \frac{\gamma_m}{2}\right) b + i\Omega_m a. \quad (\text{D.2})$$

To simplify the notation, we define operators at the boundaries of the unit cells (immediately to the left of an optomechanical element) given by $c_j = -i\sqrt{c}a_R(z_j^-)$, $d_j = -i\sqrt{c}a_L(z_j^-)$. It is also convenient to re-write the transfer matrix M_{om} in the form

$$M_{om} = \begin{pmatrix} 1 - \beta & -\beta \\ \beta & 1 + \beta \end{pmatrix}, \quad (\text{D.3})$$

with the parameter $\beta(\delta_k)$ given by

$$\beta(\delta_k) = \frac{-i\kappa_{\text{ex}}\delta_k}{-i\kappa_{\text{in}}\delta_k + 2(\Omega_m^2 - \delta_k^2)}. \quad (\text{D.4})$$

The transfer matrix M_{block} describing propagation to the next unit cell can subsequently be diagonalized, $M_{\text{block}} = SDS^{-1}$, with the diagonal matrix D given by

$$D = \begin{pmatrix} e^{iKd} & 0 \\ 0 & e^{-iKd} \end{pmatrix}. \quad (\text{D.5})$$

Physically, this diagonalization corresponds to finding the Bloch wavevectors $K(\delta_k)$ of the periodic system. The dispersion relation for the system can be readily obtained through the equation

$$\cos(K(\delta_k)d) = \cos(kd) - i\beta(\delta_k)\sin(kd). \quad (\text{D.6})$$

Writing k in terms of δ_k , we arrive at $kd = \omega_1 d/c + \delta_k d/c$. As described previously, the desirable operation regime of the system is such that the phase imparted in free propagation should be $\omega_1 d/c = (2n+1)\pi/2$. For concreteness, we set here $\omega_1 d/c = \pi/2$, satisfying this condition. For the frequencies δ_k of interest, which easily satisfy the condition $|\delta_k| \ll d/c$ and ignoring the intrinsic loss κ_{in} , the simple approximate dispersion formula

$$\cos(K(\delta_k)d) = -\frac{\kappa_{\text{ex}}\delta_k}{2(\Omega_m^2 - \delta_k^2)} \quad (\text{D.7})$$

can be found. This dispersion relation yields two bandgaps, which extend from $\pm\kappa_{\text{ex}}/2$ and $\pm 2\Omega_m^2/\kappa$, in the weakly coupled EIT regime ($\Omega_m \lesssim \kappa_{\text{ex}}$). We therefore have three branches in the band structure, with the narrow central branch having a width of $4\Omega_m^2/\kappa_{\text{ex}}$. This branch has an optically tunable width and yields the slow-light propagation.

The dispersive and lossy properties of the array can also be found by analyzing Eq. (D.6) perturbatively. Expanding Eq. (D.6) as a power series in δ_k , we find

$$K(\delta_k) = k_0 + \frac{\kappa_{\text{ex}}\delta_k}{2d\Omega_m^2} + \frac{i\kappa_{\text{ex}}\kappa_{\text{in}}\delta_k^2}{4d\Omega_m^4} + \frac{(2\kappa_{\text{ex}}^3 - 3\kappa_{\text{ex}}\kappa_{\text{in}}^2 + 12\kappa_{\text{ex}}\Omega_m^2)\delta_k^3}{24d\Omega_m^6} + O(\delta_k^4), \quad (\text{D.8})$$

which agrees with Eq. (7) in the main text.

Appendix D.2. Fractional Occupation Calculation

In our system, the Bloch functions are hybrid waves arising from the mixing of optical waveguide, optical cavity and mechanical cavity excitations. It is therefore of interest to calculate the hybrid or polaritonic properties of these waves, by studying the energy distribution of each Bloch mode.

The number of photons n_{WG} in the waveguide can be found by taking the sum of the left- and right-moving photons in a section of the device. Over one unit cell, one obtains

$$n_{\text{WG}} = (|c_j|^2 + |d_j|^2) \frac{d}{c}. \quad (\text{D.9})$$

The relation between this value and the amplitude of the hybrid Bloch wave may be found by considering the symmetry transformation used to diagonalize the unit-cell transmission matrix. Defining C_j to be the amplitude of the Bloch mode of interest, one finds $c_j = s_{11}C_j$ and $d_j = s_{21}C_j$, while from the properties of the symmetry matrix S , $|C_j|^2 = |c_j|^2 + |d_j|^2$. From here we can deduce the number of excitations in the waveguide n_{WG} , the optical cavity n_o and the mechanical cavity n_m for a given Bloch wave amplitude:

$$n_{\text{WG}} = \frac{d}{c}|C_j|^2, \quad (\text{D.10})$$

$$n_o = |a|^2 \quad (\text{D.11})$$

$$= \frac{2|\beta(\delta_k)|^2}{\kappa_{\text{ex}}}|c_j + d_j|^2 \quad (\text{D.12})$$

$$= \frac{2|\beta(\delta_k)|^2}{\kappa_{\text{ex}}}|s_{11} + s_{21}|^2|C_j|^2, \quad (\text{D.13})$$

$$n_m = |b|^2 \quad (\text{D.14})$$

$$= \frac{|\Omega_m|^2}{\delta_k^2 + \gamma_i^2/4}|a|^2. \quad (\text{D.15})$$

We then define the fractional occupation in the mechanical mode by $n_m/(n_{\text{WG}} + n_o + n_m)$ (with analogous definitions for the other components). These relations were used to plot the fractional occupation and colored band diagrams shown in the main text.

Appendix D.3. Pump Input Power

The technicalities associated with pumping the optomechanical crystal array system are subtly distinct from those in its atomic system analogue. Due to the periodic nature of the structure and its strongly coupled property ($\kappa_{\text{ex}} \gg \kappa_{\text{in}}$), a bandgap in the waveguide will arise at the frequency of the “tuning” or pump cavities. This prevents these cavities from being resonantly pumped via light propagating in the waveguide. This problem may be circumvented by making the pump frequency off-resonant from ω_2 (but still at $\omega_1 - \omega_m$), and by for example changing the splitting $\omega_1 - \omega_2$ to be less than the mechanical frequency. Interestingly, the periodic nature of the system also allows one to suppress attenuation of the pump beam through the waveguide (which would cause inhomogeneous driving of different elements along the array). Here we calculate the waveguide input powers required to drive the pump cavities. We then find the effect of the cavity dissipation rate κ_{in} on the beam intensity, to provide estimates for the power drop-off as a function of distance propagated in the system. Finally we note that there is a trade-off between required pump intensity and pump power drop-off. In other words, by tuning the pump beam to a frequency closer to the pump cavity resonance, the required input power is reduced, but the attenuation per unit cell $\exp(-\text{Im}\{K\}d)$ is increased.

To calculate the waveguide input power, we start by considering the *net* photon

flux in the right moving direction,

$$\Phi_R = |c_j|^2 - |d_j|^2. \quad (\text{D.16})$$

Using the properties of the Bloch transformation matrix S and equation (D.13), this expression may be written in terms of the number of photons in the optical cavity of interest ($n_{o,j}$),

$$\Phi_R = \frac{\kappa_{\text{ex}}}{2\beta_1^2} \frac{|s_{11}|^2 - |s_{21}|^2}{|s_{11} + s_{21}|^2} n_{o,j}, \quad (\text{D.17})$$

where

$$\beta_1(\delta_k) = \frac{-i\kappa_{\text{ex}}/2}{-i\kappa_{\text{in}}/2 - \delta_k}. \quad (\text{D.18})$$

The required input power $P_{\text{in}} = \hbar\omega_o\Phi_R$ for the system parameters studied in the main text is shown in figure 4.

To find the attenuation per unit cell $\exp(-\alpha)$, with $\alpha = \text{Im}\{K(\delta_k)\}d$, of this pump beam, we use a perturbative approach similar to that used to find the polaritonic band dispersion. By expanding the Bloch-vector as $K(\delta_k) = k^{(0)} + k^{(-1)}/\delta_k + k^{(-2)}/\delta_k^2 \dots$ and using equation (D.6), we find $k^{(-1)} = \kappa_{\text{ex}}/2d$, and $k^{(-2)} = i\kappa_{\text{ex}}\kappa_{\text{in}}/4d$ implying that $\alpha \approx \kappa_{\text{ex}}\kappa_{\text{in}}/4\delta_k^2$. This approximate expression is shown along with the exact calculated values for the attenuation in figure 4.

Appendix E. Implementation in an Optomechanical Crystal

For the theoretical demonstration of our slow-light scheme, we confine ourselves to a simplified model of an optomechanical crystal where only the two-dimensional Maxwell equations for TE waves and the equation of elasticity for in-plane deformations of a thick slab are taken into account. These equations approximate fairly accurately the qualitative characteristics of in-plane optical and mechanical waves in thin slabs, and become exact as the slab thickness is increased. In this way, many of the intricacies of the design of high- Q photonic crystal cavities (which are treated elsewhere [34]) may be ignored, and the basic design principles can be demonstrated in a slightly simplified system.

The two-dimensional optomechanical crystal (2DOMC) system used here utilizes the “snowflake” design [34], which provides large simultaneous photonic and phononic bandgaps in frequency. Here we choose to use optical wavelengths in the telecom band, *i.e.*, corresponding to a free-space wavelength of $\lambda \approx 1.5 \mu\text{m}$. For this wavelength, we found that the crystal characterized by a lattice constant $a = 400 \text{ nm}$, snowflake radius $r = 168 \text{ nm}$, and width $w = 60 \text{ nm}$, shown in figure 2, should work well.

Appendix E.1. Optical and Mechanical Cavities

Appendix E.1.1. Single Cavity System We begin our design by focusing on the creation of a single optomechanical cavity on the 2DOMC, with one relevant optical and

mechanical mode. This cavity is formed by creating a point defect, consisting of two adjacent removed holes (a so-called “L2” cavity). We calculate the optical and mechanical spectra of this cavity using COMSOL, a commercial FEM package, and find a discrete set of confined modes. Of these, one optical and one mechanical mode were chosen, exhibiting the most promising value of the opto-mechanical coupling strength g (see below for calculation). These modes are shown in figure 2(b) and (c), and were found to have frequencies $\nu_m = 11.2$ GHz and $\nu_o = 199$ THz, respectively.

Appendix E.1.2. Double Cavity System From here we move to designing the nearly-degenerate double optical cavity system with large cross-coupling rates. As two separate L2 cavities are brought close to one another, their interaction causes the formation of even and odd optical and mechanical super-modes with splittings in the optical and mechanical frequencies. This splitting may be tuned by changing the spacing between the cavities. We take the even and odd optical modes of this two-cavity system as our optical resonances at ω_2 and ω_1 .

Appendix E.1.3. Optomechanical Coupling Rates The optomechanical coupling arises from a shift in the optical frequency caused by a mechanical deformation. Our Hamiltonian for the single cavity system can then be written as

$$\hat{H} = \hbar\omega(\hat{x})\hat{a}^\dagger\hat{a} + \hbar\omega_m\hat{b}^\dagger\hat{b}, \quad (\text{E.1})$$

where $\hat{x} = x_{\text{ZPF}}(\hat{b}^\dagger + \hat{b})$ is the quantized displacement of the mechanical mode, and x_{ZPF} is the characteristic per-phonon displacement amplitude. The deformation-dependent frequency $\omega(\hat{x})$ may be calculated to first order in \hat{x} using a variant of the Feynman-Hellman perturbation theory, the Johnson perturbation theory [38], which has been used successfully in the past to model optomechanical crystal cavities [9, 39]. The Hamiltonian is then given to first order by

$$\hat{H} = \hbar\omega_o\hat{a}^\dagger\hat{a} + \hbar\omega_m\hat{b}^\dagger\hat{b} + \hbar g(\hat{b}^\dagger + \hat{b})\hat{a}^\dagger\hat{a}, \quad (\text{E.2})$$

where ω_o is the optical mode frequency in absence of deformation and

$$g = \frac{\omega_o}{2} \sqrt{\frac{\hbar}{2\omega_m d_s}} \frac{\int dl (\mathbf{Q} \cdot \mathbf{n}) \left(\Delta\epsilon |\mathbf{E}^\parallel|^2 - \Delta(\epsilon^{-1}) |\mathbf{D}^\perp|^2 \right)}{\sqrt{\int dA \rho |\mathbf{Q}|^2} \int dA \epsilon |\mathbf{E}|^2}. \quad (\text{E.3})$$

Here \mathbf{E} , \mathbf{D} and \mathbf{Q} are the optical mode electric field, optical mode displacement field and mechanical mode displacement field, respectively, d_s is the thickness of the slab, and $\epsilon(r)$ is the dielectric constant.

These concepts can be extended to optically multi-mode systems, represented by the Hamiltonian

$$\hat{H} = \hbar \sum_i \omega_{o,i} \hat{a}_i^\dagger \hat{a}_i + \hbar \omega_m \hat{b}^\dagger \hat{b} + \frac{\hbar}{2} \sum_{i,j} g_{i,j} (\hat{b}^\dagger + \hat{b}) \hat{a}_i^\dagger \hat{a}_j, \quad (\text{E.4})$$

where now the cross-coupling rates can be calculated by the following expression:

$$g_{i,j} = \frac{\omega_{i,j}}{2} \sqrt{\frac{\hbar}{2\omega_m d_s}} \frac{\int dl (\mathbf{Q} \cdot \mathbf{n}) \left(\Delta \epsilon \mathbf{E}_i^{\parallel*} \cdot \mathbf{E}_j^{\parallel} - \Delta(\epsilon^{-1}) \mathbf{D}_i^{\perp*} \cdot \mathbf{D}_j^{\perp} \right)}{\sqrt{\int dA \rho |\mathbf{Q}|^2 \int dA \epsilon |\mathbf{E}_i|^2 \int dA \epsilon |\mathbf{E}_j|^2}}. \quad (\text{E.5})$$

We denote this expression for convenience as $g_{i,j} \equiv \langle \mathbf{E}_i | \mathbf{Q} | \mathbf{E}_j \rangle$.

For the modes of the L2 cavity shown in figures 2(b) and (c), the optomechanical coupling was calculated to be $\langle \mathbf{E} | \mathbf{Q} | \mathbf{E} \rangle / 2\pi = 489$ kHz for silicon. When two cavities are brought in the vicinity of each other, super-modes form as shown in figure 2(a). We denote the symmetric (+) and antisymmetric (−) combinations by \mathbf{E}_{\pm} and \mathbf{Q}_{\pm} . These modes can be written in terms of the modes localized at cavity 1 and 2,

$$\mathbf{E}_{\pm} = \frac{\mathbf{E}_1 \pm \mathbf{E}_2}{\sqrt{2}} \text{ and } \mathbf{Q}_{\pm} = \frac{\mathbf{Q}_1 \pm \mathbf{Q}_2}{\sqrt{2}}. \quad (\text{E.6})$$

By symmetry, the only non-vanishing coupling term involving the \mathbf{Q}_{-} (antisymmetric mechanical) mode is $\langle \mathbf{E}_{+} | \mathbf{Q}_{-} | \mathbf{E}_{-} \rangle$. Assuming that the two cavities are sufficiently separated, we can approximate $\langle \mathbf{E}_{+} | \mathbf{Q}_{-} | \mathbf{E}_{-} \rangle \approx \langle \mathbf{E} | \mathbf{Q} | \mathbf{E} \rangle / \sqrt{2}$. For the super-modes of interest, $\langle \mathbf{E}_{+} | \mathbf{Q}_{-} | \mathbf{E}_{-} \rangle / 2\pi = \hbar / 2\pi = 346$ kHz.

Appendix E.2. Properties of Snowflake Crystal Waveguides

A line defect on an optomechanical crystal acts as a waveguide for light [40, 41]. Here, the line defects used consist of a removed row of holes, with the rows above and below shifted towards one another by a distance W , such that the distance between the centers of the snowflakes across the line defect is $\sqrt{3}a - 2W$ (see figure E1(a)). The waveguide was designed such that mechanically, it would have no bands resonant with the cavity frequency (see figure E1(b)) and would therefore have no effect on the mechanical Q factors. Optically, it was designed have a single band crossing the cavity frequency (see figure E1(c)) and would therefore serve as the single-mode optical waveguide required by the proposal. The band structure of the mechanical waveguide was calculated using COMSOL [42], while for the optical simulations, MPB [43] was used.

Appendix E.3. Cavity-Waveguide Coupling

By bringing the optical waveguide near our cavity, the guided modes of the line-defect are evanescently coupled to the cavity mode, and a coupling between the two may be induced, as shown in figure E2(a). Control over this coupling rate is achieved at a coarse level by changing the distance between the cavity and waveguide, *i.e.*, the number of unit cells between them. We found a distance of 6 rows to be sufficient in placing our coupling rate κ_{ex} in a desirable range. At this point, a fine tuning of the coupling rate may be accomplished by adjustment of the waveguide width parameter W , described previously. The achievable values of κ_{ex} are plotted against W in figure E2(b). For the final design, $W = 0.135a$ is used.

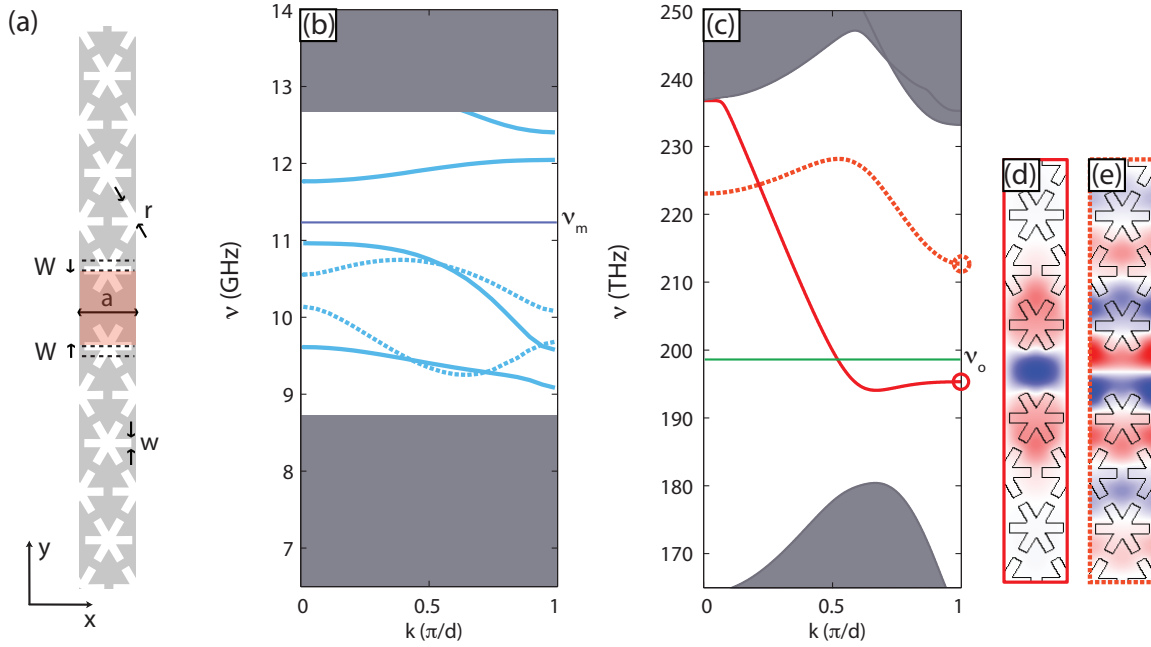


Figure E1. (a) The snowflake waveguide consists of the usual snowflake lattice, with a removed row, and adjusted waveguide width. The guiding region is shaded red for clarity. (b) The mechanical band structure exhibits a full phononic bandgap at the resonance frequency of the mechanical mode (ν_m). (c) The optical band structure exhibits a single band that passes through the resonance frequency ν_0 of the optical mode. The waveguide acts as a single-mode optical waveguide with field pattern H_z shown in (d). The H_z component of the guided optical mode of opposite symmetry is shown in (e) for completeness.

To simulate this coupling rate, we performed finite-element simulations using COMSOL where we placed the waveguide near our cavity, and placed absorbing boundaries at the ends of the waveguide away from the cavity. The resulting time-averaged Poynting vector $\langle \mathbf{S} \rangle_t = |\mathbf{E} \times \mathbf{H}^*|/2$ is plotted in figure E2(a), showing how the power flows out of the system.

Appendix E.4. Estimates for Thermoelastic Damping

The achievable storage times of our system are determined by the lifetimes of the mechanical resonances. Since we use a phononic crystal, all clamping losses have been eliminated. However, other fundamental sources of mechanical dissipation remain, and here we provide estimates for one of these, the component due to thermoelastic damping (TED) [44, 45].

Using the COMSOL finite-element solver [42], we solved the coupled thermal and mechanical equations for this system [46]. In these simulations the change in the thermal conductivity and heat capacity of silicon with temperature were taken into account. The

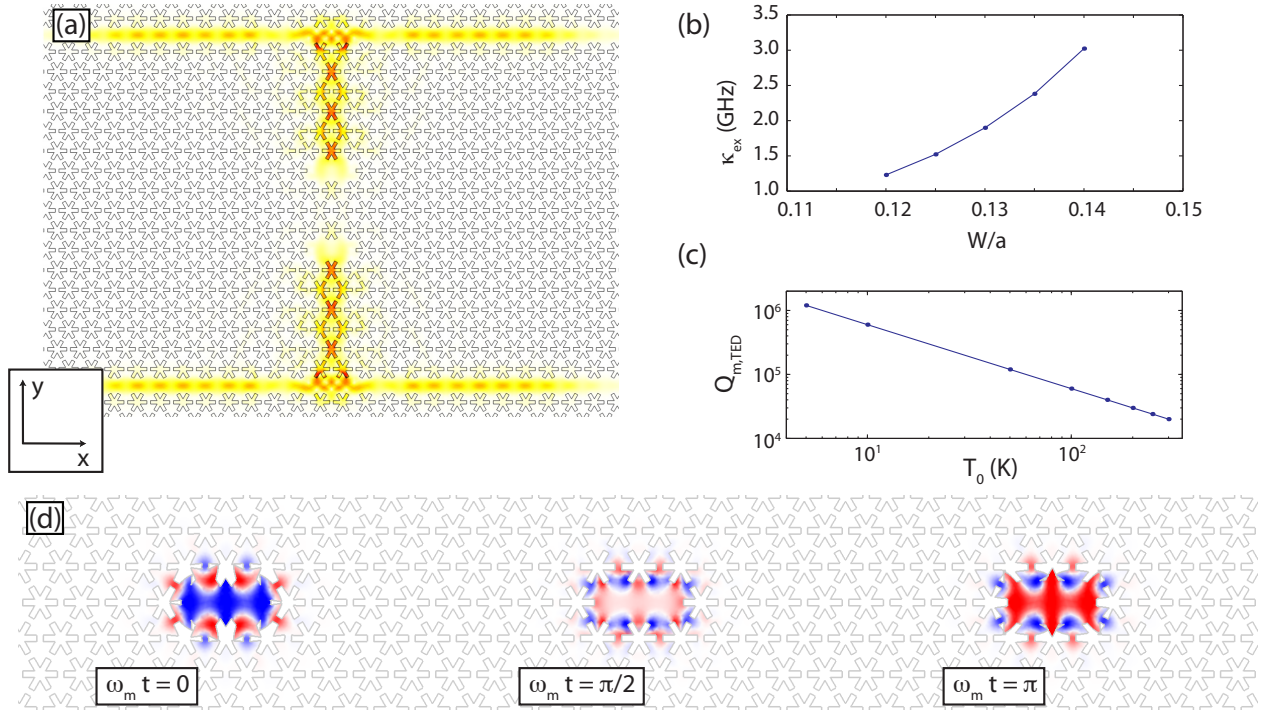


Figure E2. (a) A plot of the magnitude of the time-averaged Poynting vector, $|\langle \mathbf{S} \rangle_t|$ (in arbitrary units), shows the leakage of photons out of the double-cavity system. This induces a loss rate on the optical modes, which was used to calculate the extrinsic coupling rate κ_{ex} , plotted in (b) for various values of W/a . (c) Plot of the mechanical quality factor $Q_{\text{m,TED}}$ due to thermoelastic damping, as a function of the ambient temperature T_0 . (d) The time-harmonic component of the temperature field $\Delta T(\mathbf{r}) = T - T_0$ is plotted at various times during a mechanical oscillation period.

TED-limited quality factors, $Q_{\text{m,TED}}$ are plotted in figure E2(d). In these simulations, we see that for the mode simulated, $Q_{\text{m,TED}}$ surpasses 10^6 at bath temperatures of $T_0 < 5$ K. To illustrate some representative results of these simulations, we have plotted the change in temperature field $\Delta T(\mathbf{r})$ from the ambient temperature versus the phase of the mechanical oscillation in figure E2(d). At $\omega_m t = \pi/2$, there are variations in temperature despite the displacement field \mathbf{Q} being uniformly 0 at this time. This shows that at these frequencies, the temperature does not follow adiabatically the displacement.

Appendix E.5. Estimate for Optical Pump Heating

As mentioned in the main text, in a realistic setting the optomechanical driving amplitude Ω_m itself will be coupled to the bath temperature through absorption of optical pump photons in the tuning cavities. This optical pump heating of the structure is important in estimating the practical limits of the optomechanical system for quantum applications where thermal noise impacts system performance. As a realistic model for

the bath temperature in our proposed Silicon optomechanical crystal array, we take $T_b = T_0 + \chi\alpha^2$, where T_0 is the base temperature and χ is a temperature coefficient that describes the temperature rise in each cavity per stored cavity photon due to optical absorption. Our estimate of χ for a thin-film Silicon photonic crystal structure is as follows. The absorbed power for $|\alpha|^2$ photons stored in a cavity is given simply by $P_{loss} = \hbar\omega_o\kappa_i|\alpha|^2$, where ω_o is the resonance frequency and κ_i the optical (intrinsic) linewidth of the cavity. If we assume *all* of this power is being converted to heat, the change of temperature is $\Delta T = P_{loss}R_{th}$, where R_{th} is the effective thermal resistance of the Silicon structure. There are a number of sources in the literature for R_{th} in relevant photonic crystal geometries [47, 48]. We choose here to use the value for a two-dimensional crystal system in Silicon, $R_{th} \approx 2.7 \times 10^4$ K/W, which yields a per photon temperature rise of $\chi \sim 2 \mu\text{K}$ assuming an intrinsic loss rate of $\kappa_i \approx 4 \times 10^9$ rad/s ($Q_i \approx 3 \times 10^6$).

References

- [1] Yanik, M. F., Suh, W., Wang, Z. & Fan, S. Stopping Light in a Waveguide with an All-Optical Analog of Electromagnetically Induced Transparency. *Phys. Rev. Lett.* **93**, 233903 (2004).
- [2] Scheuer, J., Paloczi, G. T., Poon, J. K. S. & Yariv, A. Coupled Resonator Optical Waveguides: Toward the Slowing and Storage of Light. *Optics & Photonics News* **16**, 36–40 (2005).
- [3] Fleischhauer, M. & Lukin, M. D. Dark-State Polaritons in Electromagnetically Induced Transparency. *Phys. Rev. Lett.* **84**, 5094–5097 (2000).
- [4] Fleischhauer, M., Imamoglu, A. & Marangos, J. P. Electromagnetically induced transparency: Optics in coherent media. *Rev. Mod. Phys.* **77**, 633–673 (2005).
- [5] Liu, C., Dutton, Z., Behroozi, C. H. & Hau, L. V. Observation of coherent optical information storage in an atomic medium using halted light pulses. *Nature* **409**, 490–493 (2001).
- [6] Phillips, D. F., Fleischhauer, A., Mair, A., Walsworth, R. L. & Lukin, M. D. Storage of light in atomic vapor. *Phys. Rev. Lett.* **86**, 783–786 (2001).
- [7] Okawachi, Y. *et al.* All-optical slow-light on a photonic chip. *Opt. Express* **14**, 2317–2322 (2006).
- [8] Xu, Q., Dong, P. & Lipson, M. Breaking the delay-bandwidth limit in a photonic structure. *Nature Phys.* **3**, 406–410 (2007).
- [9] Eichenfield, M., Chan, J., Camacho, R. M., Vahala, K. J. & Painter, O. Optomechanical Crystals. *Nature* **462**, 78–82 (2009).
- [10] Joannopoulos, J. D., Johnson, S. G., Winn, J. N. & Meade, R. D. *Photonic Crystals: Molding the Flow of Light*, 2nd ed. (Princeton University Press, 2008).
- [11] Maldovan, M. & Thomas, E. L. Simultaneous localization of photons and phonons in two-dimensional periodic structures. *Appl. Phys. Lett.* **88**, 251907 (2006).
- [12] Notomi, M., Kuramochi, E. & Tanabe, T. Large-scale arrays of ultrahigh-Q coupled nanocavities. *Nature Photon.* **2**, 741–747 (2008).
- [13] Safavi-Naeini, A. H., Alegre, T. P. M., Winger, M. & Painter, O. Optomechanics in an ultrahigh-Q slotted 2D photonic crystal cavity. Preprint at <<http://arXiv.org/abs/1006.3964>> (2010).
- [14] Wilson-Rae, I., Nooshi, N., Zwerger, W. & Kippenberg, T. J. Theory of Ground State Cooling of a Mechanical Oscillator Using Dynamical Backaction. *Phys. Rev. Lett.* **99**, 093901 (2007).
- [15] Marquardt, F., Chen, J. P., Clerk, A. A. & Girvin, S. M. Quantum Theory of Cavity-Assisted Sideband Cooling of Mechanical Motion. *Phys. Rev. Lett.* **99**, 093902 (2007).
- [16] Arcizet, O., Cohadon, P., Briant, T., Pinard, M. & Heidmann, A. Radiation-pressure cooling and optomechanical instability of a micromirror. *Nature* **444**, 71–74 (2006).

- [17] Gigan, S. *et al.* Self-cooling of a micromirror by radiation pressure. *Nature* **444**, 67–70 (2006).
- [18] Schliesser, A., Del’Haye, P., Nooshi, N., Vahala, K. J. & Kippenberg, T. J. Radiation Pressure Cooling of a Micromechanical Oscillator Using Dynamical Backaction. *Phys. Rev. Lett.* **97**, 243905 (2006).
- [19] Cleland, A. Optomechanics: Photons refrigerating phonons. *Nature Phys.* **5**, 458–460 (2009).
- [20] Safavi-Naeini, A. H. & Painter, O. Design of Optomechanical Cavities and Waveguides on a Simultaneous Bandgap Phononic-Photonic Crystal Slab. *ArXiv e-prints* (2010). 1003.5265.
- [21] Agarwal, G. S. & Huang, S. The Electromagnetically Induced Transparency in Mechanical Effects of Light. *ArXiv e-prints* (2009). 0911.4157.
- [22] Schliesser, A. & Kippenberg, T. J. Cavity optomechanics with whispering-gallery-mode optical micro-resonators. *ArXiv e-prints* (2010). 1003.5922.
- [23] Weis, S. *et al.* Optomechanically induced transparency. Preprint at <<http://arXiv.org/abs/1007.0565>> (2010).
- [24] Safavi-Naeini, A. H. *et al.* Electromagnetically Induced Transparency and Slow Light with Optomechanics. To be submitted. (2010).
- [25] Lin, Q. *et al.* Coherent mixing of mechanical excitations in nano-optomechanical structures. *ArXiv e-prints* (2009). 0908.1128.
- [26] Gröblacher, S., Hammerer, K., Vanner, M. & Aspelmeyer, M. Observation of strong coupling between a micromechanical resonator and an optical cavity field. *Nature* **460**, 724–727 (2009).
- [27] Hong, T. *et al.* Realization of coherent optically dense media via buffer-gas cooling. *Phys. Rev. A* **79**, 013806 (2009).
- [28] Yanik, M. F. & Fan, S. Stopping and storing light coherently. *Phys. Rev. A* **71**, 110503 (2005).
- [29] Figueroa, E., Vewinger, F., Appel, J. & Lvovsky, A. I. Decoherence of electromagnetically induced transparency in atomic vapor. *Opt. Lett.* **31**, 2625–2627 (2006).
- [30] Shen, J. T. & Fan, S. Coherent photon transport from spontaneous emission in one-dimensional waveguides. *Opt. Lett.* **30**, 2001–2003 (2005).
- [31] Chang, D. E., Sørensen, A. S., Hemmer, P. R. & Lukin, M. D. Quantum optics with surface plasmons. *Phys. Rev. Lett.* **97**, 053002 (2006).
- [32] Genes, C., Vitali, D., Tombesi, P., Gigan, S. & Aspelmeyer, M. Ground-state cooling of a micromechanical oscillator: Comparing cold damping and cavity-assisted cooling schemes. *Phys. Rev. A* **77**, 033804 (2008).
- [33] Genes, C., Mari, A., Tombesi, P. & Vitali, D. Robust entanglement of a micromechanical resonator with output optical fields. *Phys. Rev. A* **78** (2008).
- [34] Safavi-Naeini, A. H. & Painter, O. Proposal for an Efficient On-Chip Phonon-Photon Translator and Applications (2010). Manuscript in preparation.
- [35] Rosenberg, J., Lin, Q. & Painter, O. Static and dynamic wavelength routing via the gradient optical force. *Nat. Photonics* **3**, 478–483 (2009).
- [36] Gardiner, C. W. & Collett, M. J. Input and output in damped quantum systems: Quantum stochastic differential equations and the master equation. *Phys. Rev. A* **31**, 3761–3774 (1985).
- [37] Meystre, P. & Sargent III, M. *Elements of Quantum Optics*, 3rd ed. (Springer-Verlag, New York, 1999).
- [38] Johnson, S. G. *et al.* Perturbation theory for maxwell’s equations with shifting material boundaries. *Phys. Rev. E* **65**, 066611– (2002). URL <http://link.aps.org/abstract/PRE/v65/e066611>.
- [39] Eichenfield, M., Chan, J., Safavi-Naeini, A. H., Vahala, K. J. & Painter, O. Modeling dispersive coupling and losses of localized optical and mechanical modes in optomechanical crystals. *Opt. Express* **17**, 20078–20098 (2009). URL <http://www.opticsexpress.org/abstract.cfm?URI=oe-17-22-20078>.
- [40] Chutinan, A. & Noda, S. Waveguides and waveguide bends in two-dimensional photonic crystal slabs. *Phys. Rev. B* **82**, 4488–4492 (2000).
- [41] Johnson, S. G., Villeneuve, P. R., Fan, S. & Joannopoulos, J. D. Linear waveguides in photonic-

- crystal slabs. *Phys. Rev. B* **62**, 8212–8222 (2000).
- [42] *COMSOL Multiphysics 3.5* (2009).
 - [43] Johnson, S. G. & Joannopoulos, J. D. Block-iterative frequency-domain methods for maxwell’s equations in a planewave basis. *Opt. Express* **8**, 173–190 (2001). URL <http://www.opticsexpress.org/abstract.cfm?URI=OPEX-8-3-173>.
 - [44] Lifshitz, R. & Roukes, M. L. Thermoelastic damping in micro- and nanomechanical systems. *Phys. Rev. B* **61**, 5600–5609 (2000).
 - [45] Zener, C. Internal friction in solids ii. general theory of thermoelastic internal friction. *Phys. Rev.* **53**, 90–99 (1938).
 - [46] Duwel, A., Candler, R., Kenny, T. & Varghese, M. Engineering mems resonators with low thermoelastic damping. *Microelectromechanical Systems, Journal of* **15**, 1437–1445 (2006).
 - [47] Barclay, P. E., Srinivasan, K. & Painter, O. Nonlinear response of silicon photonic crystal microcavities excited via an integrated waveguide and fiber taper. *Opt. Express* **13**, 801–820 (2005).
 - [48] Haret, L.-D., Tanabe, T., Kuramochi, E. & Notomi, M. Extremely low power optical bistability in silicon demonstrated using 1d photonic crystal nanocavity. *Opt. Express* **17**, 21108–21117 (2009).